Supporting Information

L-edge X-ray Absorption Spectroscopy of Dilute Systems Relevant to Metalloproteins Using a X-ray Free Electron Laser

Rolf Mitzner,[†] Jens Rehanek,[‡] Jan Kern,[§,€] Sheraz Gul,[§] Johan Hattne,[§] Taketo Taguchi,[¥] Roberto Alonso-Mori,[€] Rosalie Tran,[§] Christian Weniger,[†] Henning Schröder,[†,Π] Wilson Quevedo,[†] Hartawan Laksmono,[¶] Raymond G. Sierra,[¶] Guangye Han,[§] Benedikt Lassalle-Kaiser,[§,#] Sergey Koroidov,[Δ] Katharina Kubicek,[Σ,€] Simon Schreck,[†,Π] Kristjan Kunnus,[†,Π] Maria Brzhezinskaya,[‡] Alexander Firsov,[‡] Michael P. Minitti,[€] Joshua J. Turner,[€] Stefan Moeller,[€] Nicholas K. Sauter,[§] Michael J. Bogan,[¶] Dennis Nordlund,[$] William F. Schlotter,[€] Johannes Messinger,[Δ] Andrew Borovik,[¥] Simone Techert,[Σ,≠] Frank M. F. de Groot,[±] Alexander Föhlisch,[†,Π] Alexei Erko,[‡] Uwe Bergmann,[€,] Vittal K. Yachandra,[§,*] Philippe Wernet,[†,*] Junko Yano[§,*]*

[†]Institute for Methods and Instrumentation for Synchrotron Radiation Research, Helmholtz-Zentrum Berlin für Materialien und Energie GmbH, 12489 Berlin, Germany.

[‡]Institute for Nanometre Optics and Technology, Helmholtz-Zentrum Berlin für Materialien und Energie GmbH, 12489 Berlin, Germany.

[§]Physical Biosciences Division, Lawrence Berkeley National Laboratory, 1 Cyclotron Rd., Berkeley, CA 94720, USA.

[€]LCLS, SLAC National Accelerator Laboratory, Menlo Park, CA, USA.

[¥]Department of Chemistry, University of California-Irvine, 1102 Natural Sciences II, Irvine, CA 92697, USA.

[¶]Stanford PULSE Institute, SLAC National Accelerator Laboratory, Menlo Park, CA 94025, USA.

[#]Present address : Synchrotron SOLEIL, F-91192 Gif-Sur-Yvette, France.

[Δ]Institutionen för Kemi, Kemiskt Biologiskt Centrum, Umeå Universitet, Umeå, Sweden.

[Σ]Structural dynamics of (bio)chemical Systems, Deutsches Elektronen-Synchtrotron (DESY), Notkestrasse 85, 22607 Hamburg, Germany.

[Π]Institut für Physik und Astronomie, Universität Potsdam, 14476 Potsdam, Germany

[$]SSRL, SLAC National Accelerator Laboratory, Menlo Park, CA 94025, USA.

[≠]Max Planck Institute for Biophysical Chemistry, Am Fassberg 11, 37077 Goettingen, Germany.

[±]Inorganic Chemistry and Catalysis, Utrecht University, 3584 CG Utrecht, The Netherlands.

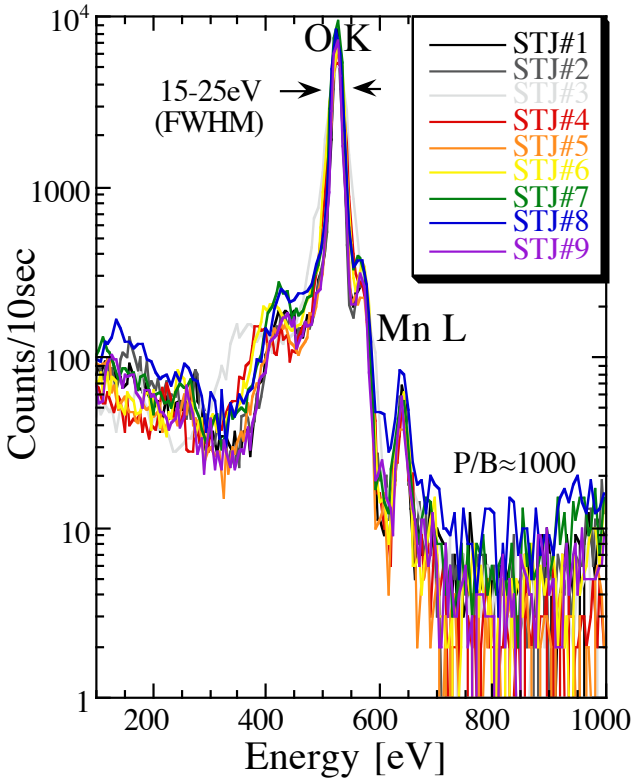

Fig. S1. The emission from a 9 channel superconducting tunnel junction detector. The emission from Mn L is a small shoulder on the intense O K emission. The sample was dehydrated to remove as much of the water as possible to reduce the signal from O. Note the log scale on the y-axis (adapted from ref. 1).

The optical layout of the reflection zone plate based partial fluorescence yield detector is displayed schematically in Fig. S3 (a). Note, for an angular resolution of different energies and diffraction orders it is required to illuminate exclusively an off-axis part of the RZP (the working area is marked red in the drawing). This allows for a straightforward discrimination of zero order light (specular reflection) and unwanted fluorescence as from the oxygen K-edge. The incident Mn fluorescence emitted from the source point is diffracted and focused at the focal plane (detector) perpendicular to the optical axis. The geometric parameters are chosen to maximize the solid angle, i.e. a close distance to the source and an optimum between “steep” incidence

angle and diffraction efficiency. The energy resolution is set to 100, sufficient to discriminate the Mn L-edge fluorescence from the overwhelming O K-edge fluorescence.

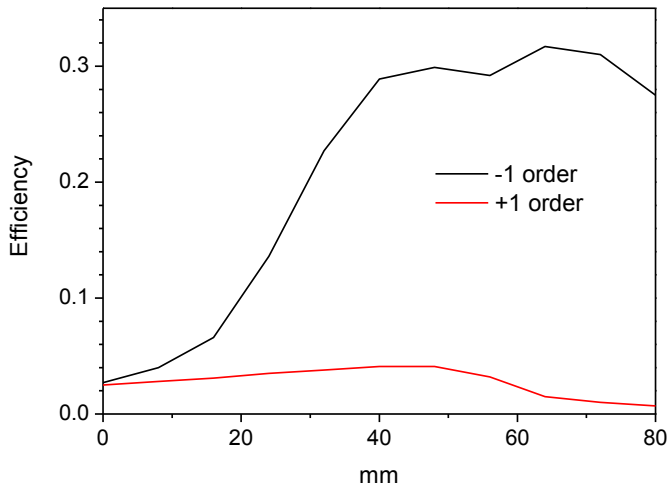

Fig. S2. Simulated diffraction efficiency along the middle of the RZP for the first negative and the first positive order.

Within the experimental conditions highest integral diffraction efficiency can be achieved for the first negative order. In Fig. S2 the efficiencies along the RZP are compared for the minus and plus first order in the middle of the structures. As a result of the larger exit angles for the plus first order the negative first order has an about seven times higher integral efficiency (ca. 16%) than the plus first order (ca. 2%).

We simulated all possible misalignments of the RZP-structure using the software Ray (2,3) to design and construct the entire setup (vacuum-chamber, detector, RZP-mount and utilized motors) around the RZP. Thus we gained information about the positioning accuracy necessary for obtaining best possible images at the CCD detector as well as best possible spectral

information from the measurements. Fig. S3 shows three resulting images (distribution of the incoming rays on the detector at the focal position of the RZP): The left panel depicts the image of a perfectly aligned setup. The middle panel shows the same plane with the zone plate shifted horizontally (orthogonal to the focal plane). The right panel illustrates the result of an angular misalignment. In this case, we simulated a rotation around the RZP normal.

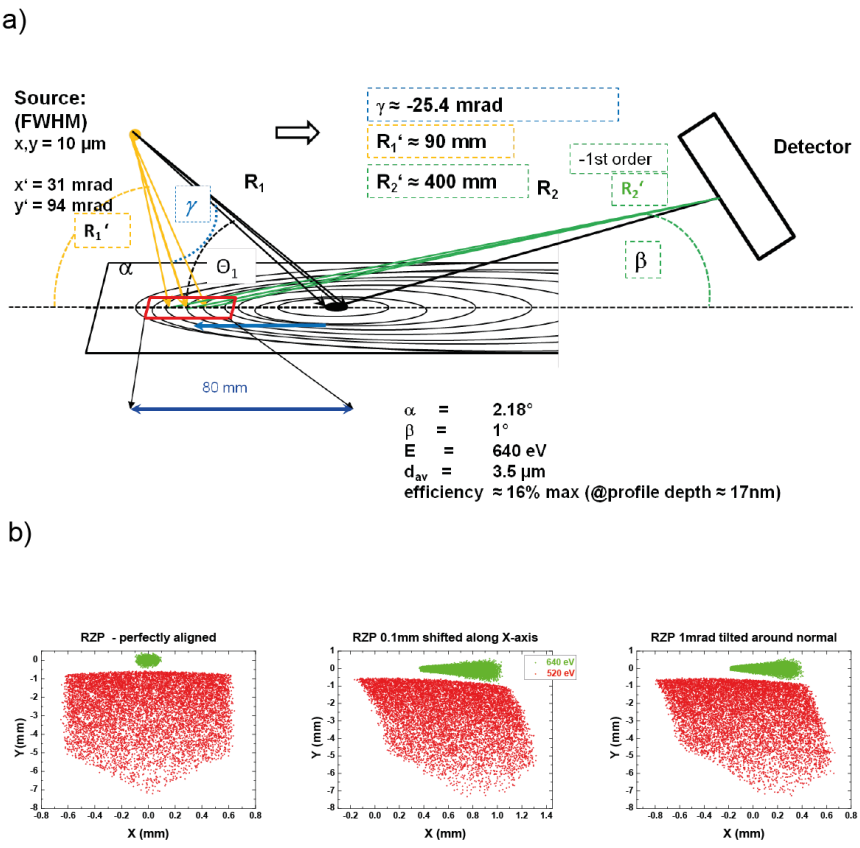

Figure S3. (a) Setup of the zone plate. The used part of the ZP structure is shown in red. (b) Distribution of incoming rays at focal position of the RZP; left: perfectly aligned, middle: shifted horizontally by 0.1 mm, right: rotated around the normal of the RZP by 1 mrad (the green spot corresponds to 640 eV, and the red area depicts 538 eV).

Four Mn L-edge absorption spectra of Mn^{2+} are compared in Fig. S4. Apparently the multiplet structure is largely independent of the chemical environment and mainly reflects the oxidation state of the Mn ions. The incident photon energies are calibrated with respect to the MnO_X sample which was calibrated with respect to MnO (4).

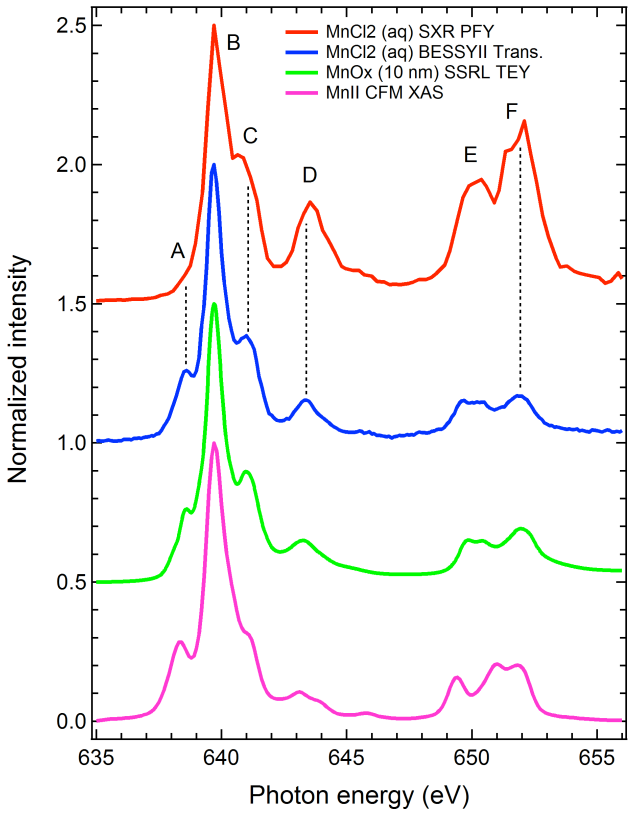

Figure S4. Comparison of L-edge absorption spectra of Mn^{2+}. From top to bottom: Mn^{2+} (aq.) from a $MnCl_2$ aqueous solution measured at SXR at LCLS in partial fluorescence yield mode (same as in Figs. 2 and 3 in the main text), Mn^{2+} (aq.) from a $MnCl_2$ aqueous solution measured at BESSYII in transmission mode (same as in Fig. 3 in the main text), thin MnO_X film (thickness 10 nm) measured at SSRL in total electron yield mode, solid MnF_2 measured in electron yield mode (taken from ref. 5). The MnO_X measurement serves as reference for calibration of the incident photon energies: The maximum of the L_3 edge was set to 639.7 eV in agreement with data in ref. 4.

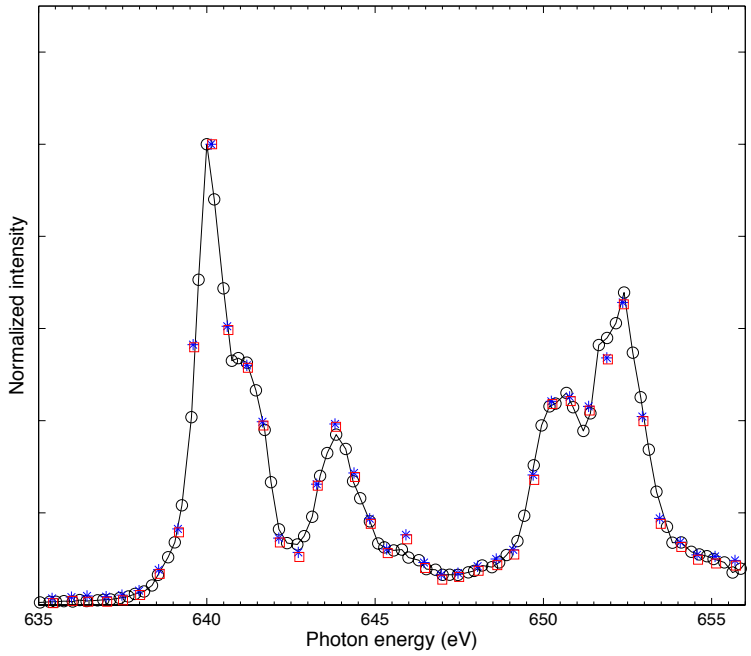

Fig. S5. Mn L-edge partial fluorescence yield (PFY) X-ray absorption spectra of $MnCl_2$ (500 mM) aqueous solution recorded at LCLS with the fluorescence-yield detector using three different experimental conditions. Photon energies were calibrated at the maximum of the L3 edge to 639.7 eV[38] with a reference spectrum of solid MnO and spectra were normalized to the peak maximum at the L3 edge. Black circles: 0.24 eV step size, 300 meV mono resolution, 20(h)×200(v) μm^2 beam size; blue stars: ~0.5 eV step size, 600 meV mono resolution, 20(h)×100(v) μm^2 beam size; red squares: ~0.5 eV step size, 417 meV mono resolution, 20(h)×40(v) μm^2 beam size.

Three different scans of the Mn L-edge are compared in Fig. S5, using different monochromator resolution, step size and beam size on the sample. The deviations between the spectra are within the noise level despite the slight changes in experimental conditions, demonstrating that we can measure L-edge spectra reproducibly with our high-transmission spectrometer.

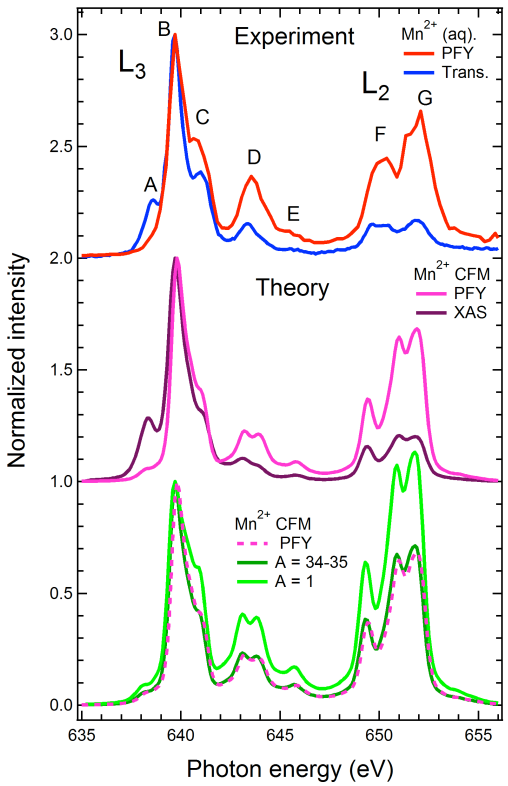

Figure S6. Top: Measured Mn L-edge partial fluorescence yield spectrum (PFY, red) and measured x-ray absorption spectrum recorded in transmission mode (Trans., blue) of Mn^{2+} (aq.). Middle: Calculated Mn L-edge PFY (pink) and x-ray absorption (XAS, violet) spectra of Mn^{2+} as calculated with the crystal-field multiplet approach (taken from ref. 6). State-dependent fluorescence and polarization effects were taken into account for the calculated PFY spectrum. Spectra in the top and middle panel are the same as in Fig. 1 and 3 of the main paper. Bottom: Calculated Mn L-edge PFY spectrum of Mn^{2+} as calculated with the crystal-field multiplet approach (dashed pink, same as in the middle) and including saturation effects with varying influence as quantified by A (small A corresponds to strong saturation, definition of A see text). All spectra are normalized to one at the maximum in the L_3 edge.

For the simulation of saturation effects (Fig. S6) we used the following formulation of the well-known formula for fluorescence-yield detected x-ray absorption:

$$I_{sat}^{PFY}(E_{in}) \propto \int \frac{I^{RIXS}(E_{in}, E_{out})}{\mu_{tot}(E_{in}) + g\mu_{tot}(E_{out})} dE_{out}$$

- I^{PFY}_{sat} is the Mn L-edge partial-fluorescence yield spectrum including saturation
- I^{RIXS} is the Mn L-edge 2p3d RIXS spectrum

- μ_{tot} is the total absorption coefficient of the sample

- g is a geometry factor defined as g = sinα/sinβ with α the angle of incidence of the x-ray beam with respect to the sample surface and β the angle of detection of the fluorescence with respect to the sample surface

We integrate the above expression over the Mn 2p3d fluorescence photon energy range. This yields a relation between I^{PFY}_{sat} and the PFY spectrum I^{PFY} without saturation. To be able to perform the integration without explicitly assuming any shape of μ_{tot} we assume that μ_{tot} is constant in the region of integration. This means that we exclude any self-absorption effects. After integration we get:

$$I_{sat}^{PFY}(E_{in}) \propto \frac{I^{PFY}(E_{in})}{\mu_{tot}(E_{in}) + g\mu_{tot}(E_{out,Mn})} = \frac{I^{PFY}(E_{in})}{\mu_{Mn}(E_{in}) + \mu_O(E_{in}) + g(\mu_{Mn}(E_{out,Mn}) + \mu_O(E_{out,Mn}))}$$

Here $E_{out,Mn}$ corresponds to a „characteristic" Mn 2p3d fluorescence energy (625 eV) and we have assumed that there are two relevant contributions to the sample absorption: Mn and O. We modify slightly the above expression to:

$$I_{sat}^{PFY}(E_{in}) \propto \frac{I^{PFY}(E_{in})}{\mu_{Mn}(E_{\max})\frac{I^{XAS}(E_{in})}{I^{XAS}(E_{\max})} + \mu_O(E_{in}) + g(\mu_{Mn}(E_{out,Mn}) + \mu_O(E_{out,Mn}))} = \frac{I^{PFY}(E_{in})}{\frac{I^{XAS}(E_{in})}{I^{XAS}(E_{\max})} + A(E_{in})}$$

E_{max} is an energy where the Mn L-edge x-ray absorption spectrum I^{XAS} is normalized to unity. Here we have selected E_{max} to be the position of the strongest absorption resonance at 640 eV (hence the label "max"). The parameter A represents the magnitude of the background absorption in the sample (relative to normalized Mn L-edge absorption). If A → infinity then

$I^{PFY}_{sat} \rightarrow I^{PFY}$. If A is close to zero or unity then one expects very strong saturation effects. A is a slowly varying function of E_{in} [due to $\mu_O(E_{in})$] and can often considered to be a constant.

With g = 1 (same angles of incidence and detection) we approximately determine a value for A of A = 34-35 for our current experimental realization. The corresponding simulation shows that the PFY spectrum is largely unaffected by saturation for A>>1. Only with an unrealistic value of A = 1 (incidence angle smaller than detection angle) do we find a strong influence of saturation.

Note in particular that self-absorption can be safely neglected as A only changes by 3% even if the Mn fluorescence spectrum would completely overlap with the Mn absorption spectrum (which it does not as the fluorescence energies are smaller than the absorption energies).

SI References

(1) Friedrich, S. Biological Applications of Cryogenic Detectors. *Nucl. Instr. & Meth. Phys. Res.* **2004,** *520*, 621-624.

(2) F. Schäfers "The BESSY Raytrace Program RAY" in Modern Developments in X-ray and Neutron Optics edited by A. Erko, Th. Krist, M. Idir, A. Michette, Berlin, Spinger, 2008, 9-39.

(3) Rehanek, J.; Schafers, F.; Erko, A.; Scheer, M.; Freund, W.; Grunert, J.; Ozkan, C.; Molodtsov, S. Simulations of Diagnostic Spectrometers for the European XFEL Using the Ray-Trace Tool RAY. *SPIE* **2011,** *8141*, 814109-814124.

(4) Gilbert, B.; Frazer, B. H.; Belz, A.; Conrad, P. G.; Nealson, K. H.; Haskel, D.; Lang, J. C.; Srajer, G.; De Stasio, G. Multiple Scattering Calculations of Bonding and X-ray

Absorption Spectroscopy of Manganese Oxides. *J. Phys. Chem. A* **2003,** *107*, 2839-2847.

(5) Cramer, S. P.; Degroot, F. M. F.; Ma, Y.; Chen, C. T.; Sette, F.; Kipke, C. A.; Eichhorn, D. M.; Chan, M. K.; Armstrong, W. H.; Libby, E., et al. Ligand-Field Strengths and Oxidation-States from Manganese L- Edge Spectroscopy. *J. Am. Chem. Soc*. **1991**, *113*, 7937-7940.

(6) Kurian, R.; Kunnus, K.; Wernet, P.; Butorin, S. M.; Glatzel, P.; de Groot, F. M. F. Intrinsic Deviations in Fluorescence Yield Detected X-Ray Absorption Spectroscopy: the Case of the Transition Metal L-2,L-3 Edges. *J. Phys. Cond. Mat*. **2012,** *24*, DOI: 10.1088/0953-8984/24/45/452201.